Inorganic Chemistry

Article

pubs.acs.org/IC

Copper Chalcogenide Clusters Stabilized with Ferrocene-Based Diphosphine Ligands†

Chhatra B. Khadka,‡ Bahareh Khalili Najafabadi,‡ Mahdi Hesari,‡ Mark S. Workentin,*,‡,§ and John F. Corrigan*,‡,§

‡Department of Chemistry, The University of Western Ontario, London, Ontario, Canada N6A 5B7

§Centre for Advanced Materials and Biomaterials Research, The University of Western Ontario, London, Ontario, Canada N6A 3K7

Supporting Information

ABSTRACT: The redox-active diphosphine ligand 1,1′-bis(diphenylphosphino)-ferrocene (dppf) has been used to stabilize the copper(I) chalcogenide clusters $[Cu_{12}(\mu_4\text{-}S)_6(\mu\text{-dppf})_4]$ (**1**), $[Cu_8(\mu_4\text{-}Se)_4(\mu\text{-dppf})_3]$ (**2**), $[Cu_4(\mu_4\text{-}Te)(\mu_4\text{-}\eta^2\text{-}Te_2)(\mu\text{-dppf})_2]$ (**3**), and $[Cu_{12}(\mu_5\text{-}Te)_4(\mu_8\text{-}\eta^2\text{-}Te_2)_2(\mu\text{-dppf})_4]$ (**4**), prepared by the reaction of the copper(I) acetate coordination complex (dppf)CuOAc (**5**) with 0.5 equiv of $E(SiMe_3)_2$ (E = S, Se, Te). Single-crystal X-ray analyses of complexes **1**−**4** confirm the presence of $\{Cu_{2x}E_x\}$ cores stabilized by dppf ligands on their surfaces, where the bidentate ligands adopt bridging coordination modes. The redox chemistry of cluster **1** was examined using cyclic voltammetry and compared to the electrochemistry of the free ligand dppf and the corresponding copper(I) acetate coordination complex **5**. Cluster **1** shows the expected consecutive oxidations of the ferrocene moieties, Cu^I centers, and phosphine of the dppf ligand.

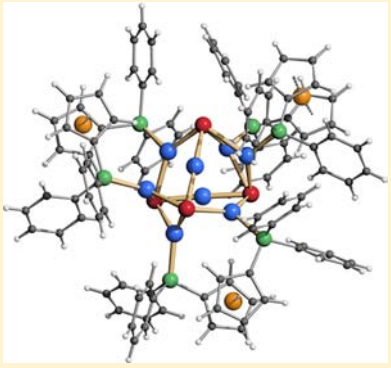

INTRODUCTION

The metalloligand 1,1′-bis(diphenylphosphino)ferrocene (dppf) has received significant research interest over last 4 decades in part because of its redox properties and flexible coordination ability when ligated to metal centers.[1] The inherent properties of this ferrocene-containing ligand can be further manipulated by forming polyferrocenyl assemblies on transition-metal clusters, whereby its electrochemical properties may be altered because of the metal−metal interactions between the ferrocenyl unit and cluster metal centers.

The intrinsic skeletal flexibility of the dppf ligand is manifest through ring twisting and tilting, making it a valuable ligand in transition-metal cluster chemistry.[1b,c,2] As such, it has been extensively utilized in cluster synthesis, most notably in the field of carbonyl cluster chemistry. Although dppf has not found similar widespread use in high-nuclearity metal chalcogen cluster chemistry,[2] structurally characterized complexes such as $[(\mu\text{-}Au_2dppf)\{S(Au_2dppf)_2]^{2+}$, $[Au_5(C_6F_5)_2(\mu_3\text{-}SC_6F_5)_2(\mu\text{-dppf})_2]^{3+}$, $[Ag_4Mo_2S_8(\mu\text{-dppf})_2]$, $[Au_6Se_2(\mu\text{-dppf})_3]^{2+}$, and $[Ni_6(\mu_3\text{-}Se_2)(\mu_4\text{-}Se_3)(dppf)_3]^{2+}$ illustrate the potential for this flexible ligand to stabilize larger metal chalcogenide frameworks.[3] Indeed, dppf has been shown to play an integral role in other branches of materials chemistry.[4] In principle, dppf, like other tertiary phosphine ligands, could be used to stabilize nanoscopic assemblies of metal chalcogen materials[5] but with the added redox property that may ultimately be tailored and developed for the generation of functional materials.[4,6]

Recent research interests have focused on the incorporation of multiple ferrocenyl units on the surface of the semiconductor metal chalcogenide clusters via the design of ferrocene-based chalcogenolate ligands.[7] To this end, the use of silylated chalcogen reagents [$E(SiMe_3)_2$ and Fc-R-ESiMe$_3$, where E = S, Se, R = spacer, and Fc = ferrocenyl] for the formation of structurally characterized ferrocenyl passivated copper and silver chalcogen clusters has been well established.[7] In principle, the "ancillary" phosphine and related ligands used to prepare nanoscopic metal chalcogenides can also be used to introduce redox functionality onto these group 11 clusters. Herein, we report a probe of the utility of the bidentate phosphine-based ferrocene ligand for the surface passivation of copper chalcogen frameworks with the synthesis and characterization of the clusters $[Cu_{12}(\mu_4\text{-}S)_6(\mu\text{-dppf})_4]$ (**1**), $[Cu_8(\mu_4\text{-}Se)_4(\mu\text{-dppf})_3]$ (**2**), $[Cu_4(\mu_4\text{-}Te)(\mu_4\text{-}\eta^2\text{-}Te_2)(\mu\text{-dppf})_2]$ (**3**), and $[Cu_{12}(\mu_5\text{-}Te)_4(\mu_8\text{-}\eta^2\text{-}Te_2)_2(\mu\text{-dppf})_4]$ (**4**), each prepared from [CuOAc-(dppf)] (**5**).

EXPERIMENTAL SECTION

All experimental procedures were performed using standard double-manifold Schlenk-line techniques under an atmosphere of dried nitrogen gas or in nitrogen-filled gloveboxes. The nonchlorinated solvents [tetrahydrofuran (THF) and pentane] were dried and collected using a MBraun MB-SP Series solvent purification system with tandem activated alumina (THF) and an activated alumina/copper redox catalyst (pentane).[8] Chlorinated solvents ($CDCl_3$, $CHCl_3$, and CH_2Cl_2) were dried and distilled over P_2O_5. Spectral-grade solvent CH_2Cl_2 was purchased from Caledon. dppf was purchased from Alfa and used as supplied. The reagents $E(SiMe_3)_2$ (E = S, Se, Te)[9] and CuOAc[10] were synthesized using literature

Received: October 8, 2012
Published: May 24, 2013

   dx.doi.org/10.1021/ic3021854 | Inorg. Chem. 2013, 52, 6798−6805

Scheme 1. Synthesis of 1−4

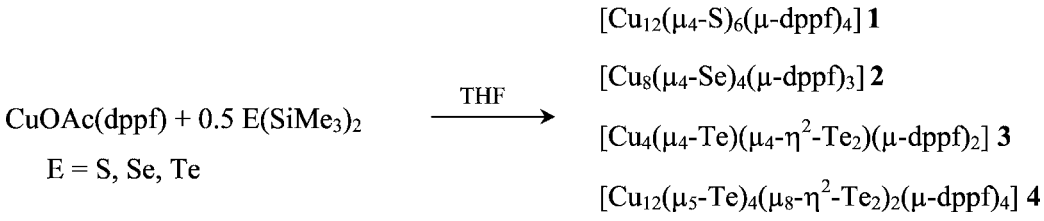

procedures. Room temperature UV−visible absorption spectra were recorded on a Varian Cary 100 spectrometer. Solution ^{1}H NMR spectra were recorded on a Varian Mercury 400 spectrometer with an operating frequency of 400.08 MHz and referenced externally to $SiMe_4$ and internally to the residual proton peak in $CDCl_3$. $^{31}P\{^1H\}$ NMR spectra were recorded on the same instrument at 161.96 MHz and were externally referenced to 85% H_3PO_4. Elemental analysis was performed by Laboratoire d'Analyze Élementaire de l'Université de Montréal, Montréal, Canada, and Chemisar Laboratories, Guelph, Canada.

An Autolab30 electrochemical workstation was equipped with *GPES 4.9* software used for cyclic voltammetry (CV) experiments. A homemade glassy carbon (GC; Tokai GC-20) working electrode (3 mm in diameter) was prepared by polishing over silicon carbide papers (500, 1200, 2400, and 4000) and then over diamond pastes (Struers; 1 and 0.25 μm). The GC electrodes were stored in ethanol and always polished before each set of experiments with a 0.25 mm diamond paste, rinsed with dry ethanol (Commercial Alcohols), sonicated in dry ethanol for 5 min and dried. Ag/AgCl (immersed silver wire in 0.1 M tetramethyl chloride) and a platinum wire served as the reference and counter electrodes, respectively.

The electrochemical samples were prepared in the glovebox using dry dichloromethane (DCM) containing 0.1 M recrystallized tetrabutylammonium perchlorate (TBAP) as the supporting electrolyte. Prior to each electrochemical experiment, the solution was saturated with argon gas for 10 min, and the inert atmosphere was kept for all CV measurements.

Single-crystal X-ray data were collected on Enraf-Nonius Kappa CCD (**1** and **4**) and Bruker APEX-II CCD (**2**, **3**, and **5**) diffractometers equipped with graphite-monochromated Mo Kα (λ = 0.71073 Å) radiation. Single crystals of the complexes were carefully selected, immersed in paraffin oil and mounted on MiteGen micromounts. Crystals were placed immediately in a cold stream of dinitrogen to minimize desolvation. The structures were solved using direct methods and refined by the full-matrix least-squares procedure of *SHELXTL*.[11] All non-hydrogen cluster atoms were refined anisotropically, while hydrogen atoms were kept at their calculated distances and refined using a riding model. For chiral **1**, the *TWIN* command in *SHELXTL* was used to refine the racemic twinning [refined Flack parameter = 0.51(2)]. Crystallographic data for structural analyses have been deposited with the Cambridge Crystallographic Data Centre, CCDC 871936 and 871937 for compounds **1** and **2** and CCDC 904597−904599 for **3**−**5**. Copies of this information may be obtained free of charge from The Director, CCDC, 12 Union Road, Cambridge CB2 1EZ, U.K. [fax (int. code) +44(1223) 336-033 or e-mail deposit@ccdc.cam.ac.uk or http://www.ccdc.cam.ac.uk].

Synthesis of 1. CuOAc (0.059g, 0.481 mmol) was dissolved in 20 mL of THF by the addition of dppf (0.267g, 0.482 mmol), and the yellow solution was cooled to −75 °C. $S(SiMe_3)_2$ (0.05 mL, 0.241 mmol) was added to the yellow solution at −75 °C. The solution changed color to pale orange after stirring for 2 h, while the reaction temperature warmed to −10 °C. Red crystals were obtained after ca. 24 h by storing the reaction solution at −25 °C. Single-crystal X-ray-quality crystals were obtained within 2 days by redissolving crystals in $CHCl_3$ and layering with pentane at room temperature. Yield: 0.10 g (80%). ^{1}H NMR ($CDCl_3$, 23 °C): δ_H 7.70 (32H, m, Ph), 7.44−7.32 (48H, m, Ph), 4.38 (16H, s, Cp), 4.20 (16H, s, Cp). $^{31}P\{^1H\}$ NMR (C_6D_6, 23 °C): δ_p −17.4 (s). Anal. Calcd for $C_{136}H_{112}Fe_4P_8S_6Cu_{12}$: C, 51.49; H, 3.56; S, 6.06. Found: C, 51.39; H, 3.37; S, 6.16.

Synthesis of 2. CuOAc (0.065g, 0.530 mmol) was dissolved in 20 mL of THF by the addition of dppf (0.294g, 0.530 mmol), and the yellow solution was cooled to −75 °C. $Se(SiMe_3)_2$ (0.06 mL, 0.265 mmol) was added to the yellow solution at −75 °C. The solution changed color to red-orange after stirring for 2 h, while the reaction temperature warmed to −10 °C. Red crystals were obtained after ca. 24 h by storing the reaction solution at −25 °C. Single-crystal X-ray-quality crystals were obtained within a few days by dissolving the crystals in CH_2Cl_2 and layering with pentane at room temperature. Yield: 0.10 g (60%). ^{1}H NMR ($CDCl_3$, 23 °C): δ_H 7.67 (24H, m, Ph), 7.43−7.36 (36H, m, Ph), 4.37 (12H, s, Cp), 4.18 (12H, s, Cp). $^{31}P\{^1H\}$ NMR (C_6D_6, 23 °C): δ_p −20.4 (s). Anal. Calcd for $C_{102}H_{84}Fe_3P_6Se_4Cu_8$: C, 49.21; H, 3.40. Found: C, 49.27; H, 3.29.

Synthesis of 3 and 4. CuOAc (0.045g, 0.367 mmol) was dissolved in 20 mL of THF by the addition of dppf (0.205g, 0.367 mmol), and the yellow solution was cooled to −75 °C. $Te(SiMe_3)_2$ (0.06 mL, 0.185 mmol) was added to the yellow solution at this temperature. The solution changed color to dark red after stirring for 1 h, while the reaction temperature warmed to −50 °C. The reaction solution was slowly warmed to room temperature and stirred for an additional 30 min to obtain a reddish-brown solution. The reaction solution was stored at −25 °C for 2 days. Highly solvated, single X-ray-quality crystals of **3** were obtained within a few days by layering with hexanes at room temperature. Yield: 0.030 g (20%) based on CuOAc. After the formation of **3**, the crystals were isolated from the mother liquor. Single X-ray-quality crystals of **4** formed within a few days at room temperature from the reaction solution. Yield: 0.035 g (20%) based on CuOAc. ^{1}H NMR for **3** ($CDCl_3$, 23 °C): δ_H 7.73 (16H, m, Ph), 7.43−7.35 (24H, m, Ph), 4.36 (8H, s, Cp), 4.19 (8H, s, Cp). $^{31}P\{^1H\}$ NMR for **3** (CD_2Cl_2, 23 °C): δ_p −19.3 (s). Anal. Calcd for $C_{68}H_{56}Fe_2P_4Te_3Cu_4$: C, 46.78; H, 3.23. Found: C, 46.80; H, 3.15. ^{1}H NMR for **4** (CD_2Cl_2, 23 °C): δ_H 7.73 (32H, m, Ph), 7.44−7.36 (48H, m, Ph), 4.38 (16H, s, Cp), 4.20 (16H, s, Cp). $^{31}P\{^1H\}$ NMR (CD_2Cl_2, 23 °C): δ_p −20.2 (s). Anal. Calcd for $C_{136}H_{112}Cu_{12}Fe_4P_8Te_8$: C, 40.82; H, 2.82. Found: C, 40.60; H, 2.56.

Synthesis of 5.[12] CuOAc (0.030g, 0.245 mmol) was dissolved in 20 mL of THF by the addition of dppf (0.136g, 0.245 mmol), and the yellow solution was obtained after stirring for 15 min at room temperature. Yellow crystals were obtained after ca. 24 h by storing the reaction solution at −25 °C. Yield: 0.140 g (85%). ^{1}H NMR ($CDCl_3$, 23 °C): δ_H 7.70 (8H, m, Ph), 7.37 (12H, m, Ph), 4.30 (4H, s, Cp), 4.19 (4H, s, Cp), 2.13 (3H, s, OAc). $^{31}P\{^1H\}$ NMR ($CDCl_3$, 23 °C): δ_p −18.1 (s). Anal. Calcd for $C_{36}H_{31}FeP_2O_2Cu$·THF: C, 64.14; H, 5.25. Found: C, 63.76; H, 5.23. Single-crystal X-ray data for **5**, including a thermal ellipsoid plot, are given in the Supporting Information (Figure S1 and Table S1).

RESULTS AND DISCUSSION

Synthesis and Characterization of the Copper Chalcogenide Complexes. The reaction of the coordination complex **5**, prepared in situ, with 0.5 equiv of the chalcogenide reagent $E(SiMe_3)_2$ in THF afforded **1** and **2** as crystalline solids after storing at −25 °C for ∼24 h (Scheme 1; E = S, Se). The crystals obtained were not of X-ray-quality; however, ^{1}H NMR data indicated the formation of product with only one ferrocene

dx.doi.org/10.1021/ic3021854 | *Inorg. Chem.* 2013, 52, 6798−6805

Table 1. Crystal Data, Data Collection, and Refinement Parameters for Complexes 1−4

	$1\cdot(CHCl_3)_{10}$	$2\cdot(CH_2Cl_2)_6$	$3\cdot(OC_4H_8)_{4.5}$	$4\cdot(OC_4H_8)_9$
chemical formula	$C_{136}H_{112}P_8Fe_4S_6Cu_{12}\cdot(CHCl_3)_{10}$	$C_{102}H_{84}P_6Fe_3Se_4Cu_8\cdot(CH_2Cl_2)_6$	$C_{68}H_{56}Cu_4Fe_2P_4Te_3\cdot(OC_4H_8)_{4.5}$	$C_{136}H_{112}Cu_{12}Fe_4P_8Te_8\cdot(OC_4H_8)_9$
fw	4364.10	2996.78	2070.14	4649.63
cryst syst	tetragonal	monoclinic	monoclinic	monoclinic
space group	$P\bar{4}2(1)/c$	$P2(1)/n$	$P2(1)/c$	$C2/c$
temp (K)	150(2)	150(2)	150(2)	150(2)
a (Å)	21.4243(2)	16.7936(11)	26.451(4)	30.448(6)
b (Å)	21.4243(2)	22.2859(15)	18.553(2)	16.561(3)
c (Å)	17.8779(3)	30.1023(19)	18.152(2)	35.833(7)
β (deg)		98.220(2)	109.966(3)	101.85(3)
V (Å^3)	8205.97(18)	11150.4(13)	8372.7(18)	17684(6)
μ (mm^{-1})	2.551	3.596	2.485	3.146
Z	2	4	4	4
ρ (g cm^{-3})	1.766	1.785	1.642	1.746
reflns collected	16417	339794	135064	106455
GOF	1.081	1.097	1.070	1.211
data/param	8347/461	21522/1270	14741/830	15563/757
R1 [$I > 2\sigma(I)$]	0.0626	0.0485	0.0797	0.0896
wR2 [$I > 2\sigma(I)$]	0.1717	0.1108	0.1963	0.2670
largest diff peak and hole (e Å^{-3})	1.213 and −1.428	2.046 and −1.487	2.630 and −1.135	2.554 and −3.539

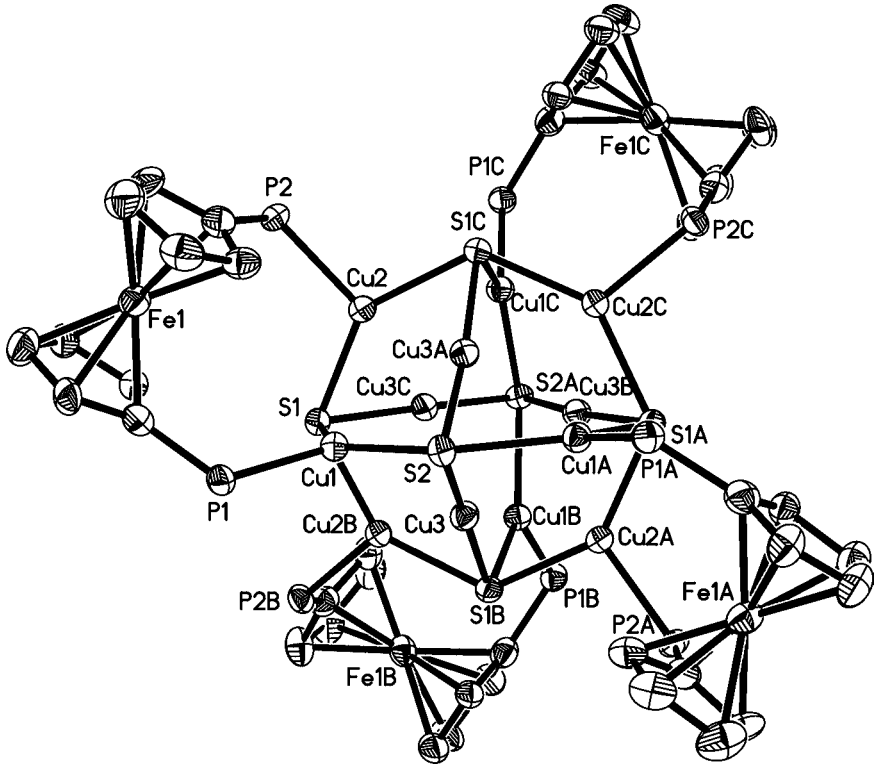

Figure 1. Molecular structure of **1**. Thermal ellipsoids are drawn at the 40% probability level. Phenyl groups and hydrogen atoms are omitted for clarity, and carbon atoms are not labeled. The molecule resides about a crystallographic $\bar{4}$ axis.

environment in solution. These NMR data obtained for **1** show a downfield shift for the protons from the phenyl groups of the free ligand, with peaks appearing as two sets of multiplets between 7.70 and 7.32 ppm. The protons from the cyclopentadienyl ring in **1** appear as broadened singlets at 4.38 and 4.20 ppm, which are again shifted slightly downfield compared to free dppf in the same solvent (4.25 and 3.99 ppm). ^{1}H NMR data obtained for **2** show a downfield shift similar to that observed for **1**, with protons from the phenyl groups appearing as multiplets between 7.67 and 7.36 ppm and protons from the cyclopentadienyl ring as broadened singlets at 4.37 and 4.18 ppm. ^{31}P{^{1}H} NMR spectra of **1** and **2** display single resonances at −17.4 and −20.4 ppm, respectively. The purity of the clusters was further confirmed by elemental analysis. Electrospray ionization mass spectrometry experiments (positive- and negative-ion modes) have been used to characterize clusters **1** and **2**. Unfortunately, only fragments were observed. Products **1** and **2** are stable as solids and in solution for an

dx.doi.org/10.1021/ic3021854 | Inorg. Chem. 2013, 52, 6798−6805

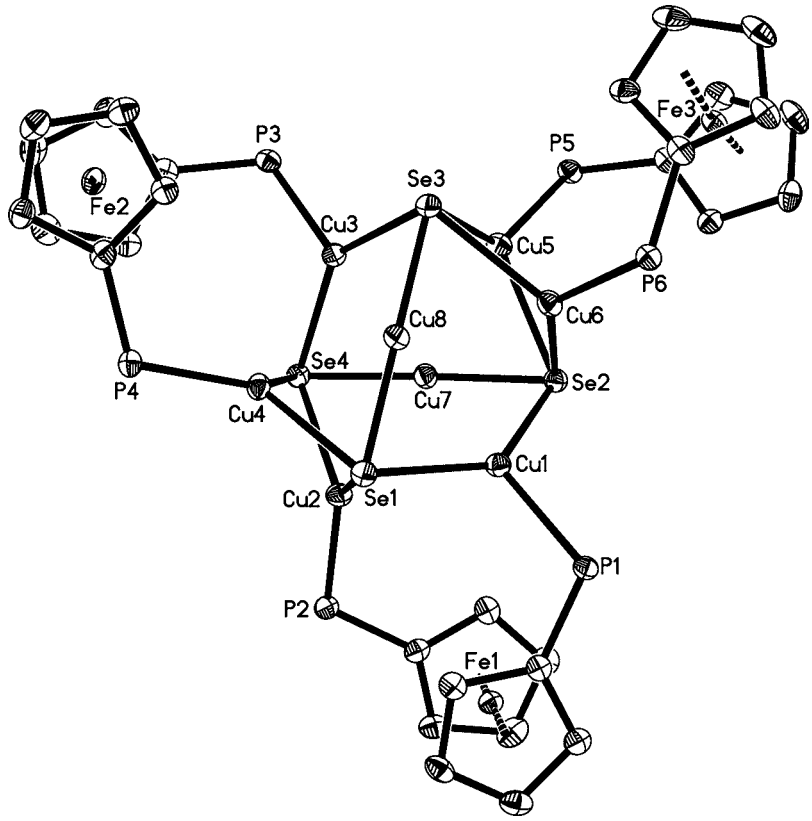

Figure 2. Molecular structure of **2**. Thermal ellipsoids are drawn at the 40% probability level. Phenyl groups and hydrogen atoms are omitted for clarity, and carbon atoms are not labeled.

extended period of time under an inert atmosphere at room temperature.

Highly solvated single crystals suitable for X-ray analysis were obtained by redissolving the red solids in either $CHCl_3$ (**1**) or CH_2Cl_2 (**2**) and layering with pentane at room temperature. Single crystals suitable for X-ray diffraction study for **3** and **4** were isolated from the layering of reaction solutions with a hydrocarbon solvent. Diffraction data were collected for all complexes, and a summary of the crystallographic, experimental, and refinement data is listed in Table 1.

The generation of $AcOSiMe_3$ is the driving force for these reactions, which leads to the formation of metal−chalcogen bonding interactions forming the copper chalcogenide cluster core, $\{Cu_{2x}E_x\}$.[5,13] The E^{2-} ligands adopt bridging coordination modes because of the high polarizabilty of these centers, which often results in the formation of polynuclear species.[13] The lighter chalcogenide ligands in **1** and **2** adopt μ_4-bridging modes exclusively. The Cu−E cores of **1** and **2** are stabilized by dppf ligands present on the surface of the complexes, which protects the cluster from decomposition and/or further condensation into bulk solids. Under similar reaction conditions, the sulfur-containing cluster **1** formed a "$Cu_{12}S_6$" core stabilized by four dppf ligands, while for the selenium-containing cluster **2**, a "Cu_8Se_4" core stabilized by three dppf ligands was obtained. The phosphorus atoms of the dppf ligands are exclusively bonded to a copper atom in a monodentate fashion in both complexes, with each acting as a bridging versus chelating ligand. The molecular structures of **1** and **2** are shown in Figures 1 and 2, respectively.

Cluster **1** crystallizes in the tetragonal space group $P\bar{4}2(1)/c$ with $Z = 2$, and there are three $CHCl_3$ solvent molecules present in the asymmetric unit. The cluster resides about a crystallographic $\bar{4}$ site, with each of the dppf ligands crystallographically equivalent. Eight of the copper centers are bonded to two sulfur and one phosphorus atoms from the dppf ligand to complete a distorted trigonal-planar coordination geometry around Cu1−Cu2C. A distorted linear coordination geometry is observed for the copper centers bonded to two sulfide ligands (Cu3−Cu3C; Figure 1). The bond angles around the three-coordinate copper atoms deviate significantly from the ideal trigonal-planar coordination angles of 120°, with smaller P−Cu−S angles ranging from 104.39(8)° to 116.19(9)° and larger S−Cu−S angles ranging from 136.07(9)° to 139.41(9)° around copper (Table 2). The bond angle around two-coordinate copper centers is 172.17(9)°. The average Cu−P bond distance in **1** is 2.292(3) Å, and the average Cu−S bond distance of 2.320(4) Å of three-coordinate copper atoms is slightly longer than that observed for the two-coordinate copper atoms [2.182(3) Å; Table 2]. For dppf, the torsion angle between the two planes formed by Fe−C−P is 98.8° and is, of course, equivalent for all four phosphine moieties in **1**. There is no short Fe···cluster contact observed in **1** or in any of the clusters reported herein.

Cu···Cu interactions in **1** vary from 2.5609(14) to 2.9235(14) Å. The molecular arrangement of the core atoms in **1** has previously been described for copper sulfide clusters containing "$Cu_{12}S_6$" with different surface ligands, namely, $[Cu_{12}S_6(PR_3)_8]$ (R = Et, ^{n}Pr, ^{n}PrPh$_2$, Et$_2$Ph).[14] This also includes structural isomers where PR_3 ligate to different copper atoms in the cluster frame than those observed in **1**. The structure of the "$Cu_{12}S_6$" core in **1** can be derived from a Cu_{12} cubeoctahedron, which is itself derived from a S_6 octahedron

dx.doi.org/10.1021/ic3021854 | Inorg. Chem. 2013, 52, 6798−6805

Table 2. Selected Bond Distances (Å) and Bond Angles (deg) for Complex 1

Cu1−S1	2.280(2)	Cu2−S1	2.304(2)
Cu1−P1	2.296(2)	Cu3−S1C	2.183(2)
Cu1−S2	2.3392(15)	Cu3−S2	2.180(2)
Cu2−P2	2.287(2)	Cu3A−S2	2.180(2)
Cu2−S1B	2.356(2)		
S1−Cu1−P1	113.90(9)	C6−P2−Cu2	115.2(3)
S1−Cu1−S2	136.07(9)	Cu3−S2−Cu1	70.63(7)
P1−Cu1−S2	110.02(10)	Cu3−S2−Cu3A	83.10(12)
P2−Cu2−S1	116.19(9)	Cu3−S2−Cu1A	76.38(8)
P2−Cu2−S1B	104.39(8)	Cu1−S2−Cu1A	135.47(14)
S1−Cu2−S1B	139.41(9)	Cu3B−S1−Cu1	107.10(9)
S2−Cu3−S1	172.17(9)	Cu3B−S1−Cu2	72.51(7)
C1−P1−Cu1	114.7(3)	Cu1−S1−Cu2	79.25(7)
Cu3B−S1−Cu2C 70.637	68.57(6)		

with 12 copper atoms bridging the sulfur atoms along these edges (Figure 1). The polyhedron is distorted because of the coordination of copper atoms to phosphorus and sulfur atoms. Copper atoms coordinated to one phosphorus and two sulfur atoms move slightly outward from the cluster center, while copper atoms coordinated to only two sulfur atoms move slightly toward the cluster core.[14b] dppf acts as a bridging ligand in **1**, where the phosphorus atoms are bonded to two alternating copper atoms that themselves lie along the edges of the S_6 octahedron. For racemic **1**, both enantiomers are observed in the unit cell (via twinning), with a refined Flack parameter of 0.51(2).

The copper selenide cluster **2** crystallizes in the monoclinic space group $P2(1)/n$ with six molecules of CH_2Cl_2. Selected bond distances for **2** are summarized in Table 3. Six copper

Table 3. Selected Bond Distances (Å) for Complex 2

Cu1−P1	2.305(2)	Cu4−Se1	2.5271(10)
Cu1−Se2	2.4271(9)	Cu5−P5	2.215(2)
Cu1−Se1	2.4343(9)	Cu5−Se3	2.4277(10)
Cu2−P2	2.2114(17)	Cu5−Se2	2.5350(10)
Cu2−Se1	2.4290(10)	Cu6−P6	2.196(2)
Cu2−Se4	2.4778(10)	Cu6−Se2	2.4083(10)
Cu3−P3	2.287(2)	Cu6−Se3	2.5526(10)
Cu3−Se3	2.4030(10)	Cu7−Se2	2.2752(9)
Cu3−Se4	2.4355(9)	Cu7−Se4	2.2869(9)
Cu4−P4	2.215(2)	Cu8−Se1	2.2737(10)
Cu4−Se4	2.4376(9)	Cu8−Se3	2.2747(10)

atoms (Cu1−Cu6) are each coordinated with one phosphorus atom from the dppf ligand and two selenium atoms to form a distorted trigonal-planar coordination geometry around the metal centers. The other two copper atoms (Cu7−Cu8) are coordinated by two selenium atoms in an almost linear fashion (Figure 2). P−Cu−Se angles range from 107.36(5)° to 132.42(5)°, and Se−Cu−Se angles range from 109.55(3)° to 138.14(4)° around the three-coordinate copper atoms. The average bond angle around two-coordinate copper centers is 176.66(6)°, which is closer to linear values than that observed in **1**. The Fe−C−P torsion angle of the dppf ligand bridging Cu1 and Cu2 is 86.9°, which for the dppf ligand bridging Cu3−Cu4 is 82.7° and that bridging Cu5−Cu6 is 106.0°, illustrating the torsional flexibility of the bidentate ligand.[1] The average Cu−P bond distance of 2.238(2) Å in **2** is similar to the Cu−P bond distance found in **1**. The range of Cu−Se bond distances for the six three-coordinate copper atoms is 2.4030(10)−2.5526(10) Å; the Cu−Se bond lengths for the two two-coordinate copper atoms are markedly shorter [avg. 2.278(4) Å]. The Cu···Cu interactions in **2** vary from 2.5021(11) to 3.0218(11) Å. The cluster **2** shares some structural features with the polynuclear copper telluride $[Cu_8Te_4(PPh_3)_7]$.[15] The molecular structure of **2** can be described as consisting of a central (nonbonded) Se_4 tetrahedron with copper bridging edges of the tetrahedron by ligating with the selenide atoms (two of the edges being doubly bridged). The dppf ligands are bonded to alternating copper atoms on the edges of the tetrahedron.

The utility of dppf in stabilizing copper−tellurium frameworks was also probed with reactions of **5** with $Te(SiMe_3)_2$. The two clusters **3** and **4** were isolated, both of which contain a mixture of telluride and ditelluride ligands in their CuTe architectures. The generation of Te_2^{2-} from $Te(SiMe_3)_2$ in CuTe cluster chemistry has been previously described and can occur when these cluster-forming reactions are brought up to room temperature.[16]

Red-brown, rapidly desolvating single crystals of **3** were obtained by layering reaction solutions with hexanes. After numerous attempts at low-temperature mounting onto a micromount, a suitable data set was obtained from a crystal displaying only modest visual signs of desolvation. Although the R(int) and final agreement factors are relatively high (Table 1), a satisfactory solution and refinement was able to be completed in the monoclinic space group $P2(1)/c$.

The structure of **3** (Figure 3 and Table 4) consists of a four-phosphine-ligated copper(I), with Cu2 and Cu3 displaying tetrahedral coordination and Cu1/Cu4 being three-coordinate. The two dppf ligands in **3** each bridge these two different copper centers. The lone telluride ligand symmetrically bridges the four copper atoms [2.539(2)−2.679(2) Å], with the μ_4-Te_2^{2-}−Cu^I bonding distances spanning a greater range of 2.554(2)−2.841(2) Å and a Te−Te bond length of 2.819(1) Å (Table 4).

The larger copper−tellurium **4** isolated contains four dppf ligands on the surface and a mixture of Te^{2-} and Te_2^{2-} ligands (Figure 4 and Table 5). In contrast to the more open framework displayed in the dodecacopper sulfide cluster **1**, the larger and more polarizable tellurium ligands in **4** result in higher coordination numbers around the copper(I) sites (3 and 4 vs 2 and 3). The telluride ligands each bridge five copper(I) atoms [2.535(2)−2.736(2) Å], and each of the tellurium sites in the Te_2^{2-} is bonded to four copper(I) atoms [2.642(2)−2.778(2) Å] with a Te−Te bond distance of 2.911(2) Å. As in **1**, the four dppf ligands bridge two copper sites, with each of these copper atoms adopting (distorted) tetrahedral coordination geometry. The other four copper atoms are each bonded to three tellurium atoms. Clusters **3** and **4** are stable as solids and in solution under an inert atmosphere at room temperature.

Room temperature (solution) UV−visible absorption spectra were recorded for solutions of dppf, **1**, and **2** and are illustrated in Figure 5. Cluster **1** displays a discrete absorption maximum around 475 nm along with a weak shoulder centered at ∼540 nm. The absorption profile for cluster **2** shows an absorption maximum at ∼540 nm and a shoulder centered at ∼460 nm. The absorptions observed at ∼475 nm (**1**) and ∼460 nm (**2**) are in a region similar to that observed for the d−d transitions in free dppf but of much stronger intensity and consistent with

dx.doi.org/10.1021/ic3021854 | Inorg. Chem. 2013, 52, 6798−6805

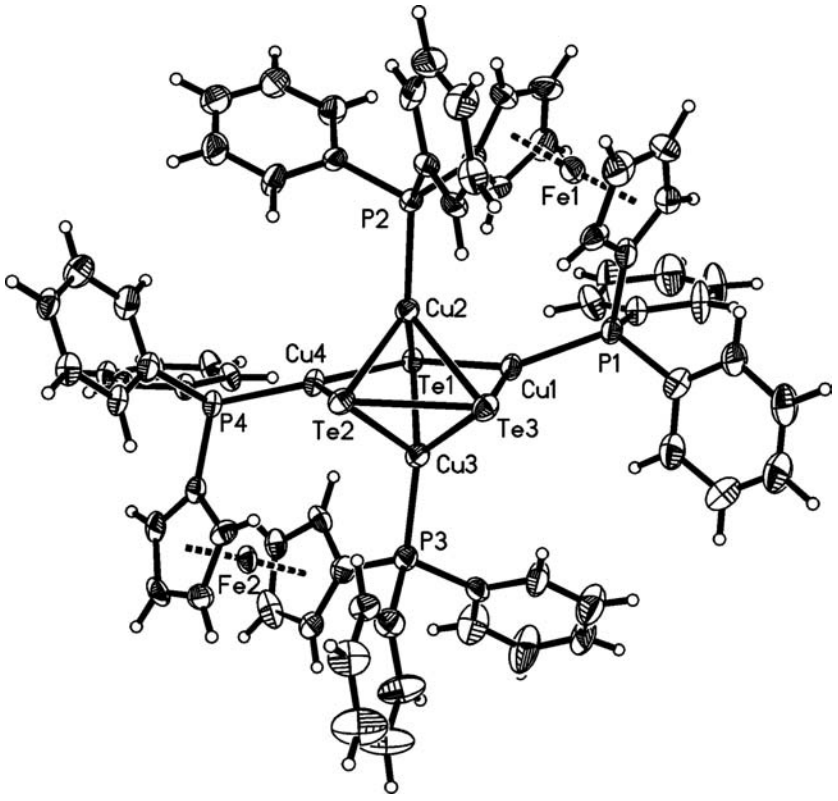

Figure 3. Molecular structure of **3**. Thermal ellipsoids are drawn at the 40% probability level.

Table 4. Selected Bond Distances (Å) for Complex 3

Cu1–Te1	2.539(2)	Cu1–Te3	2.554(2)
Cu2–Te2	2.662(2)	Cu2–Te1	2.679(2)
Cu2–Te3	2.838(2)	Cu3–Te1	2.656(2)
Cu3–Te3	2.659(2)	Cu3–Te2	2.841(2)
Cu4–Te1	2.554(2)	Cu4–Te2	2.560(2)
Te2–Te3	2.819(1)		

spectra reported for other copper(I) chalcogenide clusters (Figure 5).[15,17] The solution-state absorption data for the telluride complexes **3** and **4** display similar features but with less well-pronounced maxima (Figure S2 in the Supporting Information).

Electrochemical Study. The CV of complexes **1**–**5** was investigated in 1 mM oxygen-free DCM solutions of a complex containing 0.1 M TBAP. Parts A and B of Figure 6 show the cyclic voltammograms of **1** and **3**. The cyclic voltammograms of these two complexes show a number of similar oxidation features labeled as I–III. In order to better interpret the electrochemistry observed for these complexes, the CV of both the dppf-free ligand (Figure 6C) and CuOAc(dppf) **5** (Figure 6D) was also studied under similar conditions. The CV of the dppf-free ligand shown in Figure 6C shows a quasi-reversible one-electron oxidation with a peak potential of 1.02 V, which becomes reversible [the anodic-to-cathodic peak current ratio (I_{pa}/I_{pc}) reaches 1] with a E^0 = 0.93 V at higher scan rates (demonstrated in the figure as overlapping cyclic voltammograms, corresponding to cyclic voltammograms at increasing scan rate between 50 to 200 mV s^{-1}). This peak is assigned to oxidation of the ferrocene moiety, and its electrochemical behavior is consistent with that reported previously for the dppf ligand, where the irreversibility at lower scan rates is due to a competing electrochemical–chemical mechanism of the oxidized ferrocene ligand.[18] This is followed by additional irreversible peaks at more positive potentials (at 1.63 and 1.86 V vs Ag/AgCl) due to oxidation of the phosphorus of the phosphine ligands.[18] The electrochemistry of CuOAc(dppf) **5** (Figure 6D) shows a one-electron oxidation of the ferrocene moiety (which also becomes reversible at higher scan rates, vide

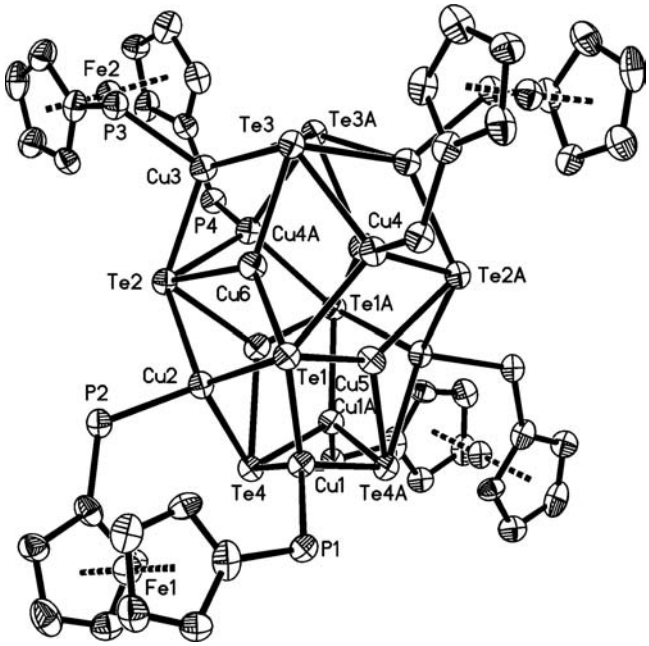

Figure 4. Molecular structure of **4**. Thermal ellipsoids are drawn at the 40% probability level. Phenyl groups and hydrogen atoms are omitted for clarity. The molecule resides about a crystallographic 2-fold rotation axis.

dx.doi.org/10.1021/ic3021854 | Inorg. Chem. 2013, 52, 6798–6805

Table 5. Selected Bond Distances (Å) for Complex 4

Te1–Cu6	2.535(2)	Te1–Cu1	2.580(2)
Te1–Cu5	2.599(2)	Te1–Cu2	2.669(2)
Te1–Cu4	2.723(2)	Te2–Cu5A	2.541(2)
Te2–Cu3	2.570(2)	Te2–Cu6	2.605(2)
Te2–Cu4A	2.666(2)	Te2–Cu2	2.736(2)
Te3–Cu6	2.642(2)	Te3–Cu3A	2.648(2)
Te3–Cu3	2.660(2)	Te3–Cu4	2.778(2)
Te3–Te3A	2.911(2)	Te4–Cu1A	2.645(2)
Te4–Cu1	2.646(2)	Te4–Cu5A	2.648(2)
Te4–Cu2	2.757(2)	Te4–Te4A	2.913(2)
Cu1–Cu5	2.623(3)	Cu1–Te4A	2.645(2)
Cu1–Cu2	2.670(3)	Cu2–Cu6	2.664(3)
Cu2–Cu5A	2.703(3)	Cu3–Cu6	2.635(3)
Cu3–Te3A	2.648(2)	Cu3–Cu4A	2.666(3)
Cu4–Te2A	2.666(2)	Cu5–Te2A	2.541(2)
Cu5–Te4A	2.648(2)		

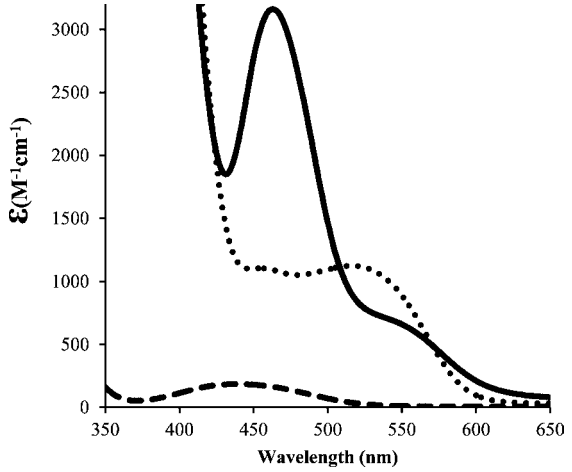

Figure 5. Room temperature (solution) UV–visible absorption spectra of clusters **1** (—), **2** (···), and dppf ligand (– –) in DCM.

infra) at 0.94 V followed by a reversible one-electron process at 1.17 V due to oxidation of the copper(I) center to copper(II).[19] Complex **5** also shows additional peaks at higher potentials due to oxidation of the phosphorus centers (not shown).

By comparing the cyclic voltammograms of compounds **1** and **3** to those measured for the dppf ligand and model copper(I) acetate complex **5**, we can better assign the redox chemistry of **1** (Figure 6A). In the case of **1** and **3**, we assign the peak labeled I to oxidation of ferrocene moieties; in the case of **1**, this has a peak potential (E_p) of 1.15 V, but it is not well-resolved from the copper oxidation because it overlaps with peak II due to oxidation of the copper(I) centers (each has their corresponding reduction peaks I′ and II′). For **3**, the first two waves are resolved enough to show the reversibility of the first due to the ferrocene moiety, which has a E_p = 1.16 and E^0 = 1.12 V vs quasi-Ag/AgCl. The peak III in each is assigned to oxidation of the phosphorus centers. In the case of **3**, there is a reduction peak at 0.36 V, which is observed only after scanning through the irreversible phosphorus oxidations (this peak also appeared in complex **4** at E_p = 0.23 V). The cyclic voltammograms of clusters **2** and **4** are similar, although the electrochemistry is not as well-resolved and difficult to reproduce because these larger clusters are less soluble and less stable, leading to electrode fouling. However, each cyclic voltammogram shows a reversible peak from the ferrocene

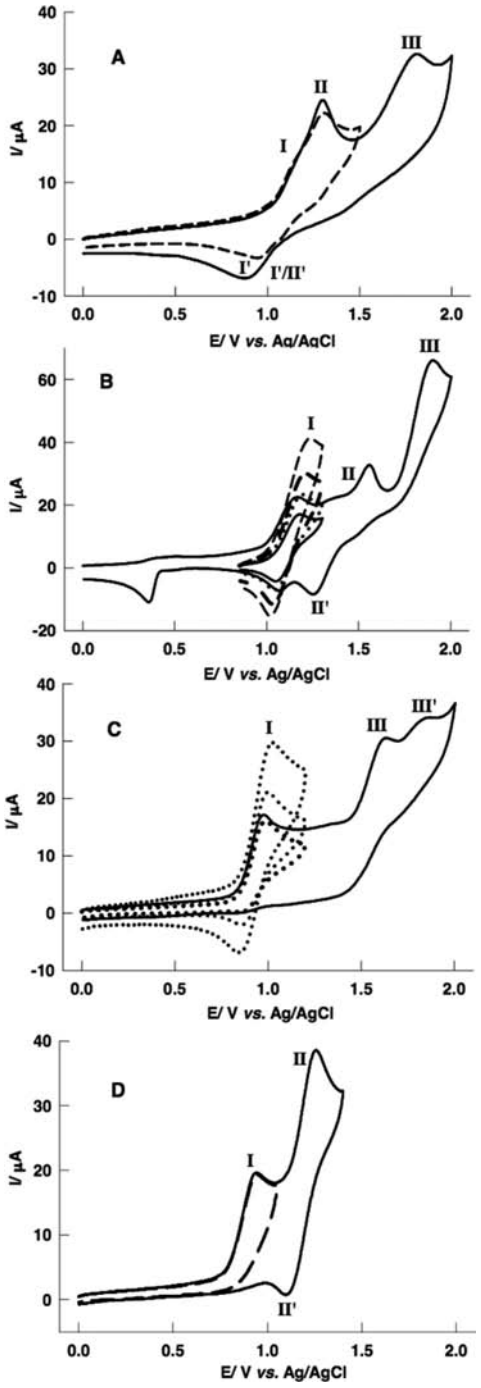

Figure 6. (A) Cyclic voltammograms of a 1 mM solution of **1** at short and wide potential range (scan rate 50 mV s^{-1}). (B) Cyclic voltammograms of a 1 mM solution of compound **3** in DCM (scan rate 50 mV s^{-1}). The reversibility of the peak I was examined by applying different scan rates: 25, 50, 100, and 200 mV s^{-1} (E^0 = 1.09 V vs Ag/AgCl). (C) Cyclic voltammograms of a 1 mM solution of the dppf ligand in a short potential window, with varying scan rates, 50, 100, and 200 mV s^{-1} (···), and a wider potential range scan rate (—), 50 mV s^{-1}. (D) Cyclic voltammograms of a 1 mM solution of complex **5** in short (– –) and wide potential (—) ranges (scan rate 50 mV s^{-1}). All experiments were done in DCM with 0.1 M TBAP. T = 25 °C.

moiety, which can overlap (appears to be more broad) because of the subsequent oxidation of the copper(I) centers. These are followed by peaks due to oxidation of the phosphorus sites

dx.doi.org/10.1021/ic3021854 | Inorg. Chem. 2013, 52, 6798–6805

(Figures S3 and S4 in the Supporting Information). No noticeable color change was observed during the electrochemical experiments.

CONCLUSION

In summary, silylated chalcogen reagents have been used to isolate copper(I) chalcogenide clusters containing multiple dppf ligands on the cluster surface. X-ray crystallographic analyses of **1**−**4** show that the dppf ligands exclusively adopt bridging coordination modes on these frameworks. CV demonstrates the consecutive oxidations of the ferrocene centers, followed by copper(I) and phosphorus, respectively.

ASSOCIATED CONTENT

Supporting Information

X-ray crystallographic data for complexes **1**−**5** in CIF format, molecular structure of **5**, crystal data of **5**, UV−visible absorption spectra, and cyclic voltammograms. This material is available free of charge via the Internet at http://pubs.acs.org.

AUTHOR INFORMATION

Corresponding Author

*E-mail: mworkent@uwo.ca (M.S.W.), corrigan@uwo.ca (J.F.C.). Phone: 1-519 661-2111 ext 86319 (M.S.W.), 1-519 661-2111 ext 86387 (J.F.C.).

Notes

The authors declare no competing financial interest.

ACKNOWLEDGMENTS

We gratefully acknowledge the Natural Sciences and Engineering Research Council of Canada for financial support of this research and equipment funding. The Government of Ontario, The University of Western Ontario, and the Canada Foundation for Innovation are thanked for equipment funding.

DEDICATION

†Dedicated to Prof. Dieter Fenske on the occasion of his 70th birthday.

REFERENCES

(1) (a) Gan, K.-S.; Hor, T. S. A. In *Ferrocenes*; Togni, A., Hayashi, T., Eds.; VCH: Weinheim, Germany, 1995; Chapter 1. (b) Fung, S.-W. A.; Hor, T. S. A. *J. Cluster Sci.* **1998**, *9*, 351. (c) Chien, S.-W., Hor, T. S. A. In *Ferrocenes: Ligands, Materials and Biomolecules*; Stepnicka, P., Ed.; John Wiley and Sons: West Sussex, England, 2008; Chapter 2.

(2) Bandoli, G.; Dolmella, A. *Coord. Chem. Rev.* **2000**, *209*, 161.

(3) (a) Crespo, O.; Canales, F.; Gimeno, M. C.; Jones, P. G.; Laguna, A. *Organometallics* **1999**, *18*, 3142. (b) Canales, F.; Gimeno, M. C.; Laguna, A.; Jones, P. G. *J. Am. Chem. Soc.* **1996**, *118*, 4839. (c) Canales, S.; Crespo, O.; Gimeno, M. C.; Jones, P. G.; Laguna, A.; Mendizabal, F. *Organometallics* **2000**, *19*, 4985. (d) Vicente, J.; González-Herrero, P.; García-Sánchez, Y.; Jones, P. G. *Inorg. Chem.* **2009**, *48*, 2060. (e) Lu, J.; Zhu, C.-C.; Li, D.-C; Dou, J.-M. *J. Cluster Sci.* **2012**, *23*, 545. (f) Kim, S. G.; Kim, D. H.; Kang, D. M.; Jabbar, M. A.; Min, K. S.; Shim, Y.-B.; Shin, S. C. *Bull. Korean Chem. Soc.* **2005**, *26*, 1603.

(4) Young, D. J.; Chien, S. W.; Hor, T. S. A. *Dalton Trans.* **2012**, *41*, 12655.

(5) Dehnen, S.; Eichhöfer, A.; Corrigan, J. F.; Fuhr, O.; Fenske, D. Synthesis and Characterization of Ib−VI Nanoclusters. In *Nanoparticles: From Theory to Application*, 2nd ed.; Schmid, G., Ed.; Wiley-VCH: New York, 2010; p 127.

(6) (a) Astruc, D.; Daniel, M.-C.; Ruiz, J. *Chem. Commun.* **2004**, 2637. (b) Daniel, M.-C.; Ruiz, J.; Nlate, S.; Blais, J.-C.; Astruc, D. *J. Am. Chem. Soc.* **2003**, *125*, 2617.

(7) (a) MacDonald, D. G.; Corrigan, J. F. *Philos. Trans. R. Soc. A* **2010**, *368*, 1455.. (b) MacDonald, D. G.; Eichhöfer, A.; Campana, C. F.; Corrigan, J. F. *Chem.—Eur. J.* **2011**, *17*, 5890. (c) MacDonald, D. G.; Kübel, C.; Corrigan, J. F. *Inorg. Chem.* **2011**, *50*, 3252. (d) Ahmar, S.; MacDonald, D. G.; Vijayaratnam, N.; Battista, T. L.; Workentin, M. S.; Corrigan, J. F. *Angew. Chem.* **2010**, *49*, 4422. (e) Ahmar, S.; Nitschke, C.; Vijayaratnam, N.; MacDonald, D. G.; Fenske, D.; Corrigan, J. F. *New J. Chem.* **2011**, *35*, 2013.

(8) Pangborn, A. B.; Giardello, M. A.; Grubbs, R. H.; Rosen, R. K.; Timmers, F. J. *Organometallics* **1996**, *15*, 1518.

(9) (a) DeGroot, M. W.; Taylor, N. J.; Corrigan, J. F. *J. Mater. Chem.* **2004**, *14*, 654. (b) So, J.; Boudjouk, P. *Synthesis* **1989**, 306.

(10) Edwards, D. A.; Richards, R. J. *J. Chem. Soc., Dalton Trans.* **1973**, 2463.

(11) (a) Sheldrick, G. M. *SHELXTL PC: An Integrated System for Solving, Refining, and Displaying Crystal Structures from Diffraction Data*, version 6.1; Bruker Analytical X-ray Systems: Madison, WI, 2000. (b) Sheldrick, G. M. *Acta Crystallogr.* **2008**, *64A*, 112.

(12) Liu, X.; Zhang, S.; Ding, Y. *J. Mol. Struct.* **2012**, *1018*, 185.

(13) (a) DeGroot, M. W.; Corrigan, J. F. In *Comprehensive Coordination Chemistry II*; Fujita, M., Powell, A., Creutz, C., Eds.; Pergamon: Oxford, U.K., 2004; Vol. 7, pp 57−123. (b) Fenske, D. In *Clusters and Colloids, From Theory to Applications*; Schmid, G., Ed.; VCH: Weinheim, Germany, 1994; pp 212−297. (c) Fenske, D.; Corrigan, J. F. In *Metal Clusters in Chemistry*; Braunstein, P., Oro, L. A., Raithby, P. R., Eds.; VCH: Weinheim, Germany, 1999; pp 1302−1324. (d) Corrigan, J. F.; Fuhr, O.; Fenske, D. *Adv. Mater.* **2009**, *21*, 1867.

(14) (a) Dehnen, S.; Schäfer, A.; Fenske, D.; Ahlrichs, R. *Angew. Chem., Int. Ed. Engl.* **1994**, *33*, 746. (b) Dehnen, S.; Fenske, D.; Deveson, A. C. *J. Cluster Sci.* **1996**, *7*, 351. (c) Dehnen, S.; Eichhöfer, A.; Fenske, D. *Eur. J. Inorg. Chem.* **2002**, 279.

(15) Eichhöfer, A.; Corrigan, J. F.; Fenske, D.; Tröster, E. *Z. Anorg. Allg. Chem.* **2000**, *626*, 338.

(16) Fenske, D.; Steck, J.-C. *Angew. Chem., Int. Ed. Engl.* **1993**, *32*, 238.

(17) (a) Corain, B.; Longato, B.; Favero, G. *Inorg. Chim. Acta* **1989**, *157*, 259. (b) Trivedi, M.; Nagarajan, R.; Kumar, A.; Rath, N. P.; Valerga, P. *Inorg. Chim. Acta* **2011**, *376*, 549.

(18) (a) Park, D.; Jabbar, M. A.; Park, H.; Lee, H. M.; Shin, S.; Shim, Y. *Bull. Korean Chem. Soc.* **2007**, *28*, 1996. (b) Nataro, C.; Campbell, A. N.; Ferguson, M. A.; Incarvito, C. D.; Rheingold, A. L. *J. Organomet. Chem.* **2003**, *673*, 47.

(19) Kuang, S. M.; Cuttell, D. G.; McMillin, D. R.; Fanwick, P. E.; Walton, R. A. *Inorg. Chem.* **2002**, *41*, 3313.